NANO LETTERS

pubs.acs.org/NanoLett Letter

Wafer-Scale Freestanding Monocrystalline Chalcogenide Membranes by Strain-Assisted Epitaxy and Spalling

Changhyeon Yoo,[▽] Han-Kyun Shin,[▽] Sang Sub Han, Seohui Lee, Chung Won Lee, Yu-Jin Song, Tae-Sung Bae, Seung Jo Yoo, Justin Cao, Jung Han Kim,* Hyo-Jong Lee,* Hee-Suk Chung,* and Yeonwoong Jung*

Cite This: *Nano Lett.* 2024, 24, 12823−12831 Read Online

ACCESS | Metrics & More | Article Recommendations | Supporting Information

ABSTRACT: Monocrystalline chalcogenide thin films in freestanding forms are very much needed in advanced electronics such as flexible phase change memories (PCMs). However, they are difficult to manufacture in a scalable manner due to their growth and delamination challenges. Herein, we report a viable strategy for a wafer-scale epitaxial growth of monocrystalline germanium telluride (GeTe) membranes and their deterministic integrations onto flexible substrates. GeTe films are epitaxially grown on Ge wafers via a tellurization reaction accompanying a formation of confined dislocations along GeTe/Ge interfaces. The as-grown films are subsequently delaminated off the wafers, preserving their wafer-scale structural integrity, enabled by a strain-engineered spalling method that leverages the stress-concentrated dislocations. The versatility of this wafer epitaxy and delamination approach is further expanded to manufacture other chalcogenide membranes, such as germanium selenide (GeSe). These materials exhibit phase change-driven electrical switching characteristics even in freestanding forms, opening up unprecedented opportunities for flexible PCM technologies.

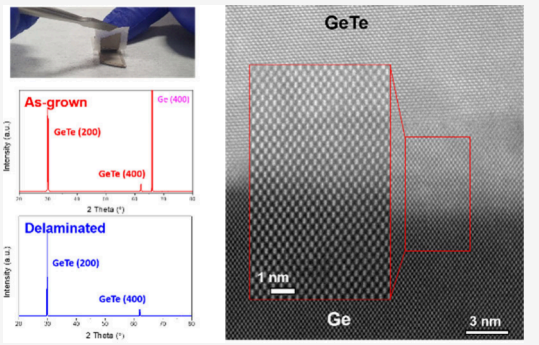

KEYWORDS: *GeTe, GeSe, Thin films, Membranes, Epitaxial growth, Ni spalling, Chalcogenide, Freestanding films, Flexible electronics, Phase change materials, PCM*

Monocrystalline thin films are essential for high-performance electronics due to their excellent charge transport properties with minimized structural imperfections,[1−3] offering opportunities for advanced device technologies.[4,5] Among a variety of methods to chemically manufacture them, the epitaxial growth method leveraging the crystallographic similarity of thin films vs growth wafers[5−7] marks a significant advancement in semiconductor industries.[3,8,9] This approach enables the growth of various electronic materials on conventional wafers in a scalable,[10] e.g., molecular beam epitaxy (MBE) for III−V compounds on silicon (Si),[11] perovskite oxides on Si,[12] and chemical vapor deposition (CVD) for two-dimensional (2D) layers on sapphire[13,14] or on silicon carbide (SiC) wafer.[15] With rapid advances in emerging technologies such as mechanically deformable electronics, epitaxial growth methods in producing high-quality monocrystalline materials accommodating various form factors have been significantly demanded.[7,10,16] While 2D layers-based membranes are easier to manipulate due to their van der Waals (vdW) bonding nature,[17−19] covalently bonded conventional thin films are difficult to fabricate in membrane forms preserving their intrinsic monocrystallinity owing to the combined challenges of their epitaxial growth and subsequent delamination.[3,20−23]

Herein, we demonstrate an epitaxial growth of high-quality monocrystalline thin films and their controlled delamination with germanium (Ge)-based chalcogenide systems, enabling the manufacture of wafer-scale membranes. Specifically, we report that Ge wafers directly reacted with vaporized tellurium (Te) precursors yield an epitaxial growth of monocrystalline germanium telluride (GeTe) thin films. The crystallographic epitaxy of GeTe vs Ge is unveiled through extensive characterizations at atomic-to-macroscopic scales. Importantly, highly localized dislocations along GeTe/Te interfaces are identified, reflecting a slight lattice mismatch between GeTe and Ge. By leveraging the dislocations accompanying high-strain gradients, we precisely delaminated GeTe thin films off their Ge wafers using a nickel (Ni) stressor-assisted spalling method. The delaminated GeTe membranes exhibit phase change-driven electrical switching characteristics, evidencing

Received: July 2, 2024
Revised: August 31, 2024
Accepted: September 30, 2024
Published: October 2, 2024

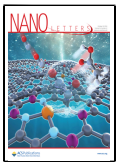

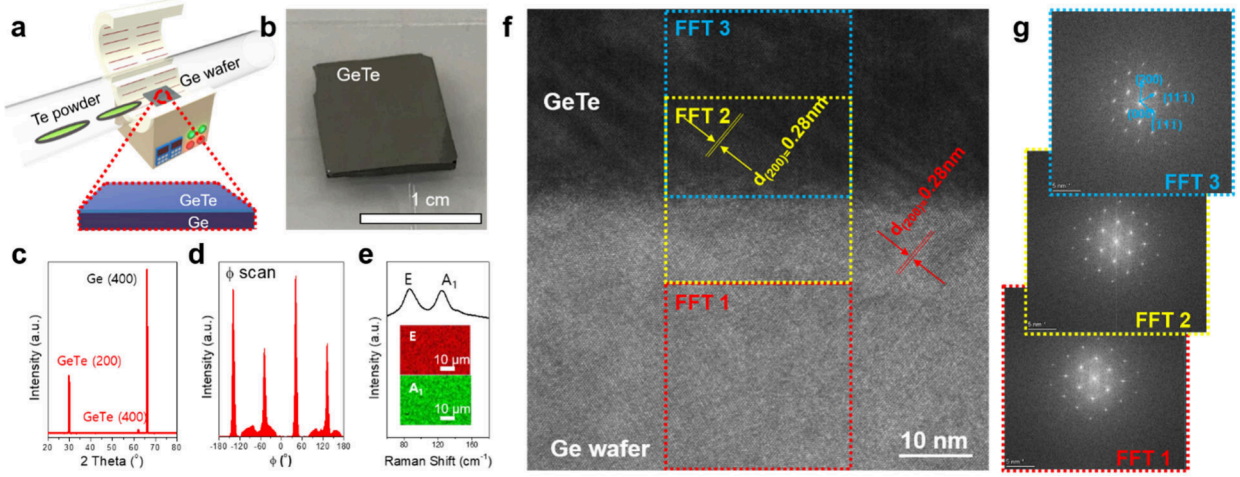

Figure 1. (a) Schematic of CVD epitaxial growth of GeTe film on Ge wafer. (b) Optical image of GeTe-grown Ge wafer. (c) Indexed XRD pattern, and (d) XRD phi (ϕ) scan of GeTe-grown Ge wafer. (e) Raman spectrum and mapping (inset) images of GeTe-grown Ge wafer. (f) Cross-sectional TEM image of GeTe/Ge interface. (g) FFT patterns obtained from respective regimes of blue, yellow, and red in (f).

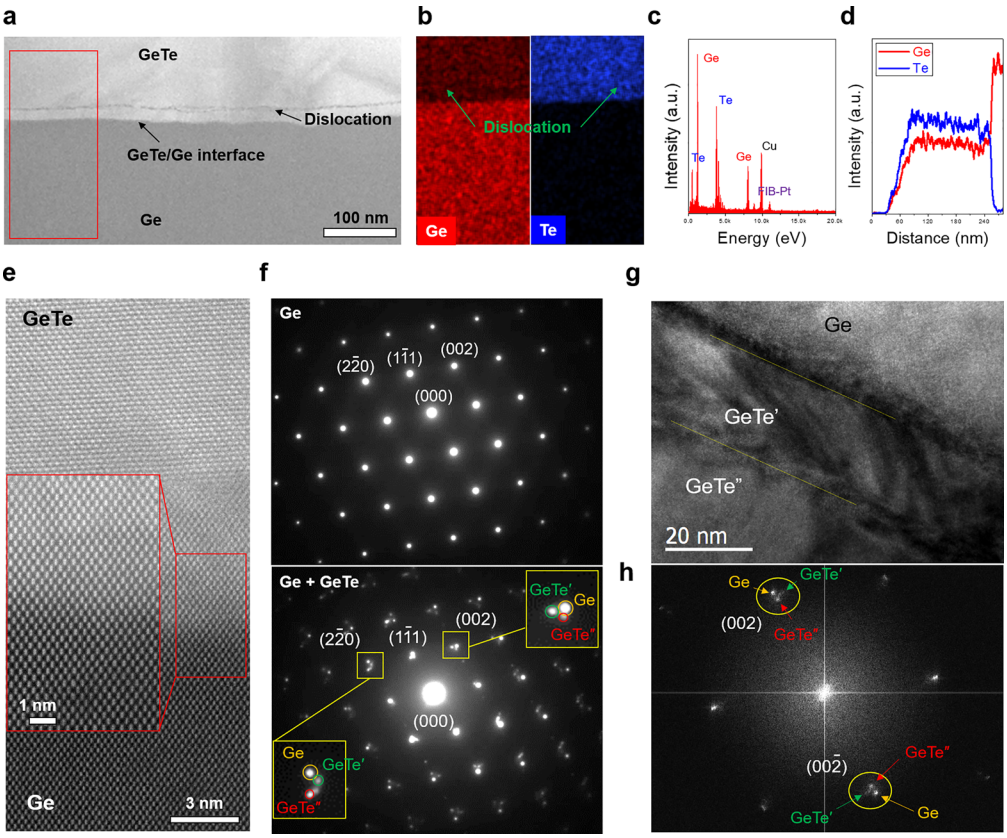

Figure 2. (a) Low-magnification cross-sectional TEM image of GeTe grown on Ge. (b) EDS mapping images corresponding to the red box in (a). (c) EDS spectrum, and (d) line scan profile obtained from GeTe. (e) Cross-sectional HR-TEM image revealing epitaxial growth of GeTe on Ge. (f) SAED patterns obtained from Ge only (top) and GeTe/Ge (bottom) regions. (g) Cross-sectional TEM image presenting Ge wafer, GeTe′ and GeTe′′ areas. (h) Diffraction spots in the FFT obtained from (g).

that this delamination method effectively preserves the structural integrity of epitaxially grown materials.

Figure 1 illustrates the CVD epitaxial growth of monocrystalline GeTe thin films on Ge wafers, which employs a direct tellurization of (100)-oriented Ge wafers with vaporized Te. Details about the CVD growth conditions are presented in the Supporting Information. Figure 1b shows an image of a wafer-scale (>cm^2) GeTe-grown-Ge wafer, which is characterized by X-ray diffraction (XRD) and Raman spectroscopy. Figure 1c presents an indexed XRD pattern obtained from a sample prepared at a CVD temperature of 350 °C. It displays only two prominent peaks at 29.9° and 62.1°, which correspond to (200) and (400) planes of cubic GeTe, respectively, while the additional peak at 65.9° matches the (400) plane of cubic Ge. The appearance of only *a*-axis aligned XRD peaks of GeTe and Ge cubic structures indicates their

https://doi.org/10.1021/acs.nanolett.4c03127
Nano Lett. 2024, 24, 12823−12831

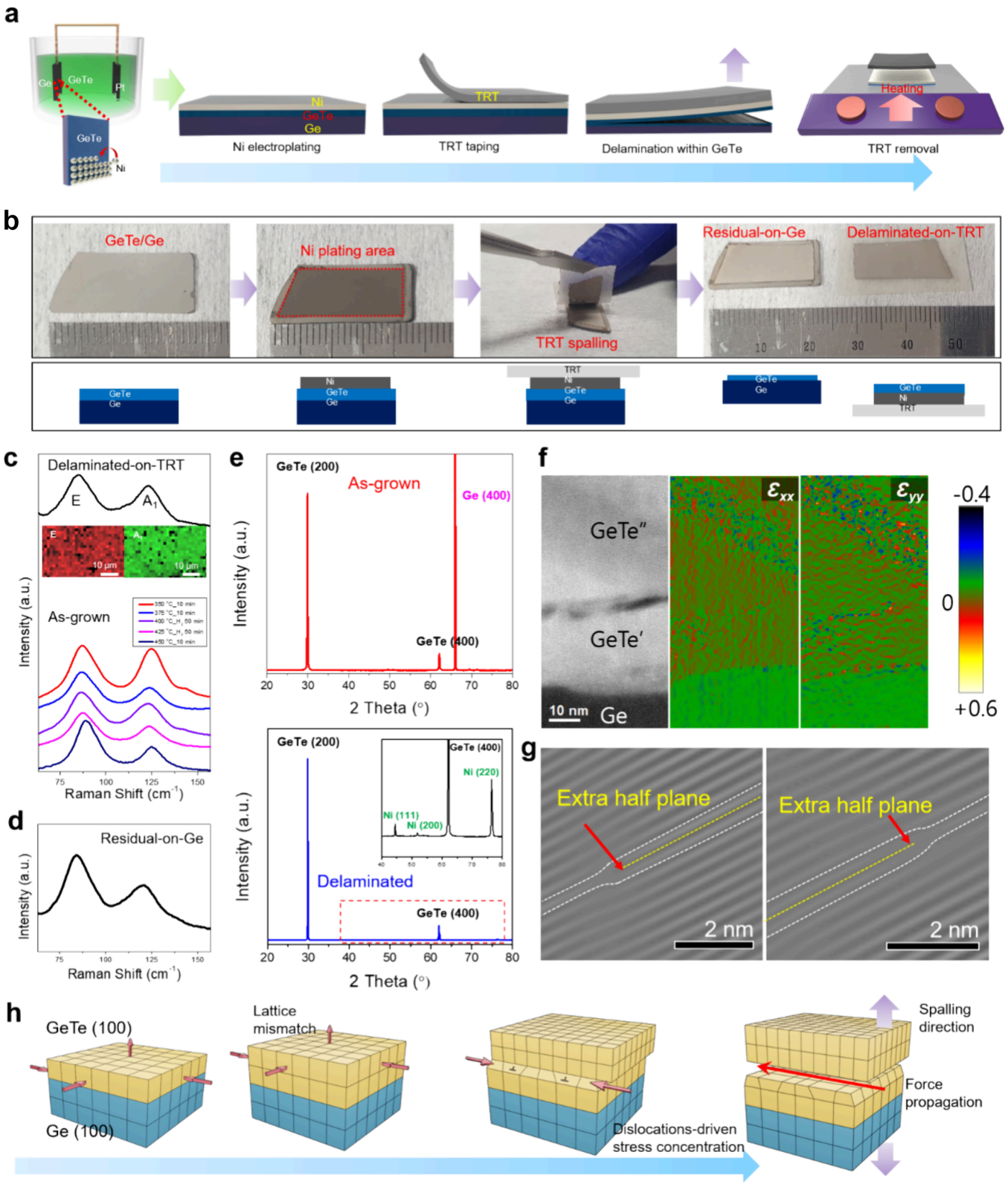

Figure 3. (a) Schematic illustration of spalling-enabled delamination of GeTe thin film. (b) Images of GeTe film delamination. (c) Comparison of Raman spectra for delaminated GeTe vs as-grown GeTe prepared at various conditions along with Raman mapping images of delaminated GeTe (inset). (d) Raman spectrum of remaining GeTe on Ge. (e) Comparison of XRD patterns for as-grown GeTe (top) vs delaminated GeTe. (f) Cross-sectional TEM image (left) and its corresponding GPA strain mapping images depicting strain distributions along *x*- (middle, ε_{xx}) and *y*- (right, ε_{yy}) orientations. (g) Direct visualization of individual dislocations existing within GeTe. (h) Schematic illustration of working principle for GeTe delamination enabled by lattice mismatch-driven concentration of strains along dislocations.

epitaxial relation, suggesting a growth of monocrystalline GeTe. Additional XRD pattern obtained from a sample grown at 450 °C is presented in Supporting Information, Figure S1, which displays a similar monocrystallinity of GeTe. It is

https://doi.org/10.1021/acs.nanolett.4c03127
Nano Lett. 2024, 24, 12823−12831

interesting to note that the grown GeTe possesses a cubic structure that is commonly achievable at much higher CVD temperatures (e.g., ∼700 K),[24−26] indicating a possible role of the cubic-phased Ge wafer in guiding the orientation of growing GeTe. Figure 1d shows the XRD phi (ϕ) scan profile obtained from the same sample, revealing four different peaks through 360° rotation. This observation confirms the cubic structure of GeTe accompanying a 4-fold rotational symmetry, while three peaks are expected to appear in rhombohedral GeTe.[27,28] Furthermore, the four peaks are observed to be evenly separated by ∼90° from one another, which indicates that the monocrystalline GeTe is epitaxially grown on the (100) Ge wafer resembling its cubic phase. Figure 1e presents Raman characteristic peaks at ∼86.7 cm^{-1} and ∼124.9 cm^{-1}, which are assigned to E and A_1 modes of GeTe, respectively, consistent with previous studies.[29−31] Further insights into the monocrystalline structure of GeTe are obtained by transmission electron microscopy (TEM) characterizations. Figure 1f displays a TEM cross-sectional image of as-grown GeTe on Ge, focusing on their interface. Both Ge and GeTe exhibit a (200) plane interplanar spacing of 0.28 nm, indicating a high degree of lattice matching, thus suggesting the epitaxial growth of GeTe on Ge through their coherent and continuous crystallographic orientations across the interface. This epitaxial relationship is predicable based on their highly comparable crystal structures (Ge: ICDD: 04-0545, GeTe: ICDD: 65-0305),[32,33] which is also consistent with the XRD observations. An enlarged view of the TEM image is presented in Supporting Information, Figure S2, which better visualizes lattice fringes across the GeTe/Ge interface. Figure 1g presents fast Fourier transform (FFT) images derived from three different areas of the HR-TEM image, i.e., Ge wafer (red box), GeTe film (blue box), and GeTe/Ge interface (yellow box). The nearly identical indexed FFT images, revealing the diffraction features of monocrystallinity, confirm the lattice coherency of the materials, directly evidencing their epitaxial relation.

With the gained insights into the monocrystalline continuity of GeTe and Ge, we focus on unveiling their epitaxial growth principle through in-depth atomic-scale studies. Figure 2a presents a low-magnification cross-sectional TEM image of as-grown GeTe on Ge, revealing their distinct image contrast. Notably, laterally aligned dislocations are observed along the GeTe/Ge interface within the GeTe region. The presence of the lateral dislocations is further verified by a TEM image taken at a higher magnification (Supporting Information, Figure S3). Figure 2b depicts a cross-sectional energy-dispersive X-ray spectroscopy (EDS) elemental mapping image acquired from the red box in Figure 2a, revealing a uniform distribution of Ge (red) and Te (blue) atoms. The EDS spectrum in Figure 2c, along with additional EDS quantification analysis presented in Supporting Information Figure S4, confirms that the as-grown GeTe films possess nearly stoichiometric atomic ratios of Ge:Te. Furthermore, the uniform distribution of Ge (red) and Te (blue) within the material is further verified by the EDS line profile in Figure 2d, which also identifies the GeTe thickness of ∼150 nm. Figure 2e shows a representative cross-sectional HR-scanning TEM (HR-STEM) image demonstrating an atomic-scale visualization of the GeTe/Ge interface along with its magnified view (red box). It reveals that the GeTe film is seamlessly interfaced with the underlying Ge wafer without a significant lattice distortion or crystallographic discontinuity, evidencing its epitaxially grown monocrystallinity. Figure 2f top presents an indexed selective area electron diffraction (SAED) pattern obtained from the Ge wafer in Figure 2e, clarifying its perfect monocrystallinity. Figure 2f bottom presents a SAED pattern obtained from a large area of the GeTe/Ge interface, exhibiting a high similarity to that of the Ge wafer. However, a careful inspection unveils intriguing features that signify the epitaxial nature of GeTe growth on Ge. For instance, around the monocrystallinity diffraction spots contributed by the Ge wafer (yellow circles within the insets), periodically located satellite spots are well resolved (green/red circles within the insets). This observation suggests a presence of slight structural variations within the GeTe film, leading us to hypothesize two distinct phases of GeTe′ (green) and GeTe′′ (red). It is worth mentioning that these distinct phases of GeTe still preserve monocrystalline characteristics despite slight variations with respect to the monocrystallinity of Ge. Figure 2g displays a cross-sectional HR-TEM image with a larger field of view, distinguishing the GeTe film into two phases: GeTe′ and GeTe′′. To identify which diffraction spots belong to which phases, we performed *in situ* FFT analysis on the HR-TEM image in a real-time manner. The FFT analysis video in Supporting Information, Movie 1 clarifies that SAED patterns sequentially transit from three different crystalline regimes of Ge, GeTe′, and GeTe′′, indicating a slight lattice mismatch between GeTe and Ge. Figure 2h presents FFT diffraction spots corresponding to Ge (orange), GeTe′ (green), and GeTe′′ (red), further supporting the epitaxial growth of GeTe on Ge resembling its monocrystallinity. These comprehensive observations suggest that the epitaxial growth of GeTe on Ge inevitably introduces structural variations into GeTe (i.e., dislocations in Figure 2a), resulting in distinct phases. Indeed, owing to the slight (6%) lattice mismatch between Ge (a = 5.67 Å) and GeTe (a = 6.01 Å),[32,33] the growth of GeTe on Ge should involve an accumulation of lattice strain which causes a formation of dislocations. The presence of these intrinsic dislocations within GeTe films plays a critical role in their controlled delamination, as discussed in the next section.

Toward exploring the intrinsic properties of monocrystalline GeTe films for unconventional applications such as flexible devices, we investigate a strategy to delaminate them off growth wafers, preserving their structural integrity. Specifically, we developed a "spalling" process; i.e., the physical separation of thin films from their growth substrates through a controlled propagation of stress-concentrated cracks within them.[22,34,35] This technique utilizes a distinctive fracture mode in brittle materials, such as semiconductor wafers, where crack propagation is controlled by externally deposited stressor materials exerting tensile stress.[36] Ni is employed as the stressor material for GeTe owing to its strong adhesion and high fracture toughness.[34−38] Following the deposition of Ni on top of a GeTe/Ge wafer, a mechanical force is applied to the wafer surface, which allows for a full delamination of the GeTe film. Figure 3a illustrates the spalling procedure for the delamination of a GeTe film conducted in the following sequences: (1) electroplating Ni deposition on GeTe/Ge, (2) attachment of thermal release tape (TRT) on Ni/GeTe/Ge, (3) exertion of pulling force on the edge of the sample, (4) removal of TRT by heating at ∼180 °C. Subsequently, a pulling force is exerted in a perpendicular orientation with respect to the GeTe film, initiating a lateral propagation of internal cracks along its strain-concentration regimes (i.e., dislocations) promoted by the externally applied sheer stress of Ni.[22,34−36] Figure 3b shows images of the sequential steps for

https://doi.org/10.1021/acs.nanolett.4c03127
Nano Lett. 2024, 24, 12823−12831

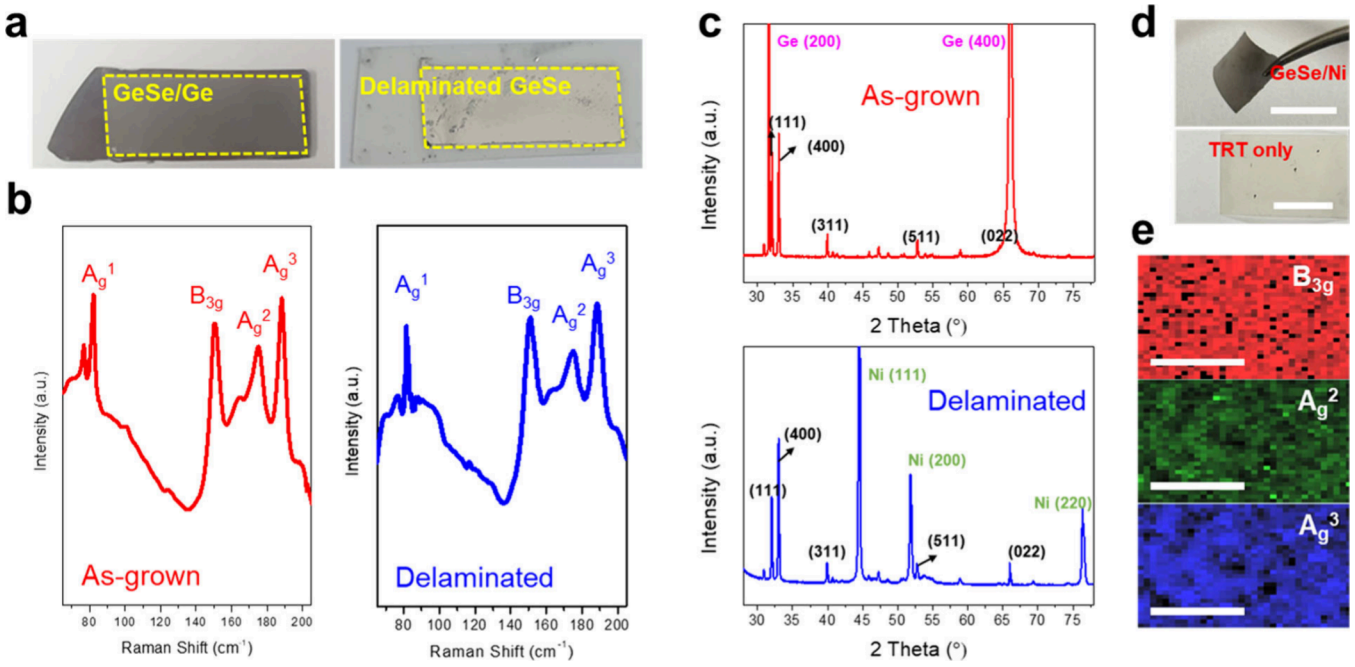

Figure 4. (a) Camera images of GeSe film grown on Ge wafer (left) and its corresponding delaminated GeSe on Ni/TRT (right). (b) Raman spectra of identical GeSe in its as-grown on Ge (left) and delaminated on Ni/TRT (right) states. (c) XRD profiles obtained from identical GeSe in its as-grown on Ge (top) and delaminated on Ni/TRT (bottom) states. (d) Camera images of GeSe/Ni (top) and removed TRT (bottom). The scale bars are 1 cm. (e) Raman mapping images of GeSe film corresponding to B_{3g}, A_g^2, and A_g^3 Raman peaks. The scale bars are 300 μm.

the spalling-enabled GeTe delamination (top column) as well as their corresponding cross-sectional illustrations of the sample prepared at each stage (bottom column). Figure 3c presents a Raman spectrum obtained from the "delaminated-on-TRT" sample in Figure 3b, alongside its corresponding mapping images (top inset). The spectrum is also compared to the Raman characteristic of as-grown GeTe/Ge samples prepared under various CVD conditions (bottom)—i.e., temperatures in a range of 350–450 °C with varying carrier gas concentrations (argon (Ar): 90–100%, and hydrogen (H_2): 10–0%). Raman peaks from the delaminated sample are located at 85 and 122 cm^{-1}, which are consistent with E and A_1 peaks of the as-grown GeTe/Ge samples, respectively, evidencing a successful delamination of GeTe. The variations in the intensity ratio of E/A_1 peaks observed in Figure 3c are attributed to the thickness difference of GeTe films resulting from varying CVD conditions.[29] Furthermore, the Raman mapping images confirm a highly homogeneous distribution of GeTe on the delaminated sample. Figure 3d presents a Raman spectrum obtained from the "residual-on-Ge" sample in Figure 3b, revealing Raman characteristics consistent with those in Figure 3c. The fact that the identical Raman characteristic peaks of GeTe are observed in both the delaminated and residual samples indicates that the spalling-enabled delamination occurs "within" GeTe rather than at the interface of GeTe/Ge. To further verify the delamination efficacy as well as the structural quality of the delaminated samples, we perform XRD characterizations with identical samples before/after the spalling process. Figure 3e compares XRD patterns obtained from an identical sample in its pristine state of GeTe/Ge (top) vs delaminated state of GeTe/Ni/TRT (bottom). Nearly identical XRD peaks corresponding to (200) and (400) cubic GeTe are observed in both states before/after the delamination. This observation strongly confirms that the delaminated GeTe sample well preserves its intrinsic monocrystallinity even after being delaminated, which is highly consistent with the characteristics of epitaxially grown GeTe in Figure 1c. The inset in Figure 3e bottom corresponds to a magnified view of the red dotted box, revealing the polycrystallinity of the electroplated Ni (ICDD: 4-0850). These comprehensive analyses suggest that the delamination is initiated within GeTe from regions of high structural variations with concentrated stresses. Based on the observation of the lattice mismatch-driven formation of dislocations within GeTe films (Figure 2a and 2g), we attempt to identify the spatial distribution of stains associated with the dislocations and quantify their amount. For this, we employ a geometric phase analysis (GPA)-based strain mapping of TEM images. Figure 3f shows a representative cross-sectional TEM image (left) and its corresponding GPA strain maps, revealing a spatial distribution of strains across the GeTe′/GeTe′′ within the GeTe film along x (ε_{xx}, middle) and y (ε_{yy}, right) orientations. Consequently, this dislocations-concentrated region accompanying a large degree of the localized strain is believed to be prone to the spalling-induced delamination. Additional HR-TEM and GPA images obtained from a different location further visualize the strain-concentrated dislocations (Supporting Information, Figure S5). Furthermore, the presence of the strain-accompanying dislocations is directly evidenced by a reverse FFT image method. Figure 3g presents reverse FFT images extracted from two different locations of the HR-TEM image in Figure 3f, revealing the existence of extra half-plane-associated dislocations. Larger views of the corresponding HR-TEM and reverse FFT images are presented in Supporting Information, Figure S6. Figure 3h provides a detailed schematic illustration of the dislocation-induced spalling delamination of a GeTe thin film off its growth wafer. Initially, the GeTe film is epitaxially grown on the wafer, introducing a certain degree of compressive stress due to their slight lattice mismatch. The thickness of the GeTe film increases as the

https://doi.org/10.1021/acs.nanolett.4c03127
Nano Lett. 2024, 24, 12823−12831

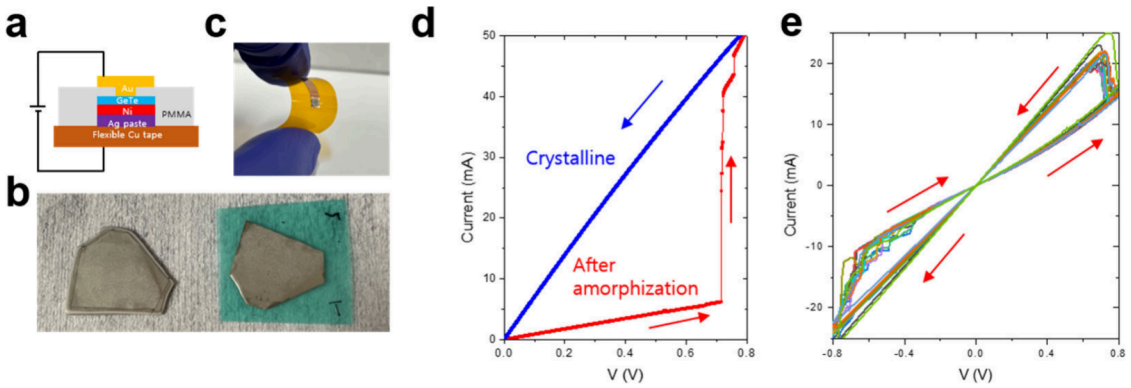

Figure 5. (a) Schematic illustration of flexible GeTe device integrated on PI. (b) Camera image of identical GeTe before (left) and after (right) delamination/integration. (c) Image of flexible GeTe device under mechanical bending. (d) *I*−*V* curves of flexible GeTe device in its crystalline state (blue) and after amorphization RESET pulse application (red). (e) Resistive switching characteristics from another sample under repetitive sweeps obtained with different SET/RESET conditions.

CVD reaction further proceeds, which intensifies the compressive stress. Sequentially, a series of dislocations are formed within the GeTe film near the GeTe/Ge interface in a way that relaxes the stress, as previously described in epitaxial growth studies.[39] The lattice imperfection around the dislocations is subjected to the upward pulling force exerted by the Ni stressor, which causes the delamination of the GeTe film accompanying the propagation of dislocations-accompanying cracks. Additionally, atomic force microscopy (AFM) characterizations were performed (Supporting Information, Figure S7), which confirms that the delaminated side of the GeTe film exhibits a much smoother surface compared to the top surface of the as-grown film, further suggesting the dislocations-initiated delamination. Furthermore, we note that the delamination efficacy is determined by complex interplays of multiple factors, such as the physical properties (e.g., thickness) of the films to be delaminated as well as the stressor layers. In-depth discussions on these factors are provided in Supporting Information.

The versatility of this wafer growth/delamination approach is applied to other covalently bonded polycrystalline chalcogenide materials grown in a nonepitaxial manner. Specifically, a nonepitaxial growth of GeSe with a larger lattice mismatch and its subsequent spalling delamination is demonstrated. Figure 4a shows images of a GeSe-grown-on Ge wafer obtained by the direct CVD selenization reaction similar to the GeTe growth (left) and its corresponding delamination of GeSe (right). Figure 4b presents Raman spectra of a GeSe film in its as-grown (left) vs delaminated (right) states, revealing identical GeSe characteristic peaks at 81.5, 149.8, 174.7, and 188.0 cm^{-1} corresponding to A_g^1, B_{3g}, A_g^2, and A_g^3, respectively, consistent with previous studies.[24,40−43] Figure 4c compares XRD characteristics of an identical GeSe sample before (top) and after (bottom) the delamination, showing indexed peaks of (111), (400), (311), (511), and (022) orthorhombic GeSe (ICDD: 48-1226).[27,44] The fact that identical peaks are observed for both states indicates that the polycrystallinity of GeSe is well preserved before/after the delamination. Figure 4d displays images of a delaminated GeSe/Ni sample in a freestanding form (top) and its corresponding remaining TRT (bottom). Figure 4e presents the Raman mapping images obtained from the B_{3g}, A_g^2, and A_g^3 modes of the same sample, revealing a high spatial homogeneity of GeSe over a large area of 700 μm × 500 μm. Additionally, we demonstrate the direct conversion of GeTe to GeSe via the CVD reaction developed in this study (Supporting Information, Figure S8), which further highlights its versatility.

Lastly, we demonstrate electrical measurements of delaminated chalcogenide films by focusing on leveraging the phase-change switching characteristics of GeTe films in flexible forms. Chalcogenide thin films are extensively employed as switching media for PCMs, which employ their electrically triggered transition between crystalline and amorphous states.[45−49] GeTe is particularly promising as a PCM component owing to its combined advantage of excellent switching speed and thermal stability.[46,50,51] Realizing such characteristics in freestanding GeTe membranes may open up opportunities for flexible PCM device applications, which remain unexplored due to a lack of suitable materials. Figure 5a illustrates a cross-sectional view of a delaminated GeTe film integrated onto a flexible polyimide (PI) substrate, where top-to-bottom electrode contacts are configured with Ni and gold (Au). Figure 5b shows a representative image of the remaining GeTe/Ge after the delamination (left) and the corresponding delaminated GeTe/Ni on TRT (right). Figure 5c displays an image of a fabricated device under mechanical bending before electrical measurements. Figure 5d illustrates the current−voltage (*I*−*V*) characteristics of the device obtained from modulated electrical pulse applications. The device initially exhibits a linear *I*−*V* curve (blue) accompanying a low resistance of ∼15.57 Ω, reflecting the monocrystallinity of the delaminated GeTe. It is then subjected to an amorphization "RESET" voltage pulse, which introduces the crystalline-to-amorphous transition into GeTe. Details for the pulse conditions are described in Supporting Information. Upon a sequential *I*−*V* sweep following the RESET process, the device initially exhibits a high resistance of ∼116.72 Ω, followed by an abrupt surge in current at a certain threshold voltage (V_{th}) of ∼0.72 V. This observation of the threshold switching indicates that the device undergoes a transition from a low resistance state (LRS) to a high resistance state (HRS) introduced by the electrical pulse-driven Joule heating.[45,52] Figure 5e shows the *I*−*V* curves of another device where the switching characteristics are modulated with different pulse conditions. Upon repetitive *I*−*V* sweeps, this device exhibits pinched hysteresis loops showing typical memristive characteristics, reflecting reversible transitions between partially crystallized and

https://doi.org/10.1021/acs.nanolett.4c03127
Nano Lett. 2024, 24, 12823−12831

amorphized phases, consistent with previous observations.[53] In between each $I-V$ sweep, the device is subjected to SET and RESET pulses for the partial crystallization and amorphization of GeTe, respectively. Pulses of 10 V amplitude and 75−100 ns duration are applied for RESET, while 5 V and 10 μs duration are for SET. The device displays well-resolved LRS and HRS over 20 sweep cycles despite the small resistance contrast between them, as well as the accompanying V_{th} of ∼0.75 V. Beyond confirming the intrinsic switching characteristics inherent to phase-change GeTe films, it is noteworthy that performances of flexible PCM devices can also be affected by externally introduced mechanical stimuli, which often alter the electronic structures of PCM materials.[54] In fact, mechanical bending can introduce defects into GeTe films as well as alter their crystalline−amorphous transition dynamics, potentially causing variations in SET/RESET voltages, switching speeds, and endurances.[54] Investigations into the correlation of these mechanical inputs vs performance parameters are believed to be essential in further improving flexible PCM devices.

In conclusion, we report a high-quality wafer-scale monocrystalline growth of GeTe thin films and their spalling-assisted delamination by utilizing the strain-accompanying epitaxial relation with Ge wafers. We identify that the delaminated GeTe films preserve their intrinsic structural and electrical characteristics even in freestanding forms, confirming the high scalability and reliability of the developed growth/delamination method. Furthermore, we clarify the specific role of the epitaxy-driven formation of dislocations in governing the delamination efficacy, as well as demonstrate the high versatility of this strain-assisted delamination approach. This study highlights promising aspects of chalcogenide membranes for unconventional device applications such as flexible PCM technologies.

■ ASSOCIATED CONTENT

Supporting Information

The Supporting Information is available free of charge at https://pubs.acs.org/doi/10.1021/acs.nanolett.4c03127.

Experimental methods, in-depth discussions on delamination factors, XRD pattern, HR-TEM images, cross-sectional TEM image, EDS quantification data, GPA strain map images, reverse FFT images, AFM topography images, camera images, and Raman spectra (PDF)

FFT analysis video (MP4)

■ AUTHOR INFORMATION

Corresponding Authors

Jung Han Kim − *Department of Materials Science and Engineering, Dong-A University, Busan 49315, Republic of Korea*; orcid.org/0000-0002-6678-2282; Email: junghankim@dau.ac.kr

Hyo-Jong Lee − *Department of Materials Science and Engineering, Dong-A University, Busan 49315, Republic of Korea*; orcid.org/0000-0003-3889-9245; Email: hyojong@dau.ac.kr

Hee-Suk Chung − *Research Center for Materials Analysis, Korea Basic Science Institute, Daejeon 34133, Republic of Korea*; Email: hschung13@kbsi.re.kr

Yeonwoong Jung − *NanoScience Technology Center, University of Central Florida, Orlando, Florida 32826, United States; Department of Materials Science and Engineering and Department of Electrical and Computer Engineering, University of Central Florida, Orlando, Florida 32816, United States*; orcid.org/0000-0001-6042-5551; Email: yeonwoong.jung@ucf.edu

Authors

Changhyeon Yoo − *NanoScience Technology Center, University of Central Florida, Orlando, Florida 32826, United States*

Han-Kyun Shin − *NanoScience Technology Center, University of Central Florida, Orlando, Florida 32826, United States; Department of Materials Science and Engineering, Dong-A University, Busan 49315, Republic of Korea*

Sang Sub Han − *NanoScience Technology Center, University of Central Florida, Orlando, Florida 32826, United States*

Seohui Lee − *NanoScience Technology Center and Department of Chemistry, University of Central Florida, Orlando, Florida 32826, United States*

Chung Won Lee − *NanoScience Technology Center, University of Central Florida, Orlando, Florida 32826, United States*

Yu-Jin Song − *Department of Materials Science and Engineering, Dong-A University, Busan 49315, Republic of Korea*

Tae-Sung Bae − *Research Center for Materials Analysis, Korea Basic Science Institute, Daejeon 34133, Republic of Korea*

Seung Jo Yoo − *Research Center for Materials Analysis, Korea Basic Science Institute, Daejeon 34133, Republic of Korea*

Justin Cao − *NanoScience Technology Center, University of Central Florida, Orlando, Florida 32826, United States; Department of Materials Science and Engineering, University of Central Florida, Orlando, Florida 32816, United States*

Complete contact information is available at: https://pubs.acs.org/10.1021/acs.nanolett.4c03127

Author Contributions

[▽]C.Y. and H.-K.S. contributed equally to this work. Y.J. conceived and directed the project. C.Y. and H.-K.S. prepared and characterized samples under the guidance of Y.J. S.L., C.W.L., and J.C. assisted in sample preparation under the guidance of H.-K.S. and Y.J. S.S.H., Y.-J.S., T.-S.B., and S.J.Y. performed structural characterizations of the samples under the guidance of J.H.K., H.-S.C., and Y.J. H.-K.S. and S.L. performed spalling delamination experiments under the guidance of H.-J.L. and Y.J. C.Y., H.-K.S., S.S.H., and Y.J. wrote the manuscript with input from all authors.

Notes

The authors declare no competing financial interest.

■ ACKNOWLEDGMENTS

Y.J. acknowledges financial support from the U.S. National Science Foundation (CAREER: 2142310). S.S.H. acknowledges financial support from the Preeminent Postdoctoral Program (P3) at UCF. H.-S.C. was supported by the Synchrotron and Electron Microscopy Program (A426200), funded by the Korea Basic Science Institute. T.-S.B. was supported by the Technology Innovation Program (20010542), funded by the MOTIE, Korea. J.H.K. acknowledges support from the Ministry of Science and ICT (Project Number: 2024-22030006-00) and the Commercialization Promotion Agency for R&D Outcomes (COMPA).

REFERENCES

(1) Zhang, Z.; Xu, X.; Qiu, L.; Wang, S.; Wu, T.; Ding, F.; Peng, H.; Liu, K. The Way towards Ultrafast Growth of Single-Crystal Graphene on Copper. *Adv. Sci.* **2017**, *4* (9), 1700087.

(2) Haque, M. A.; Troughton, J.; Baran, D. Processing-Performance Evolution of Perovskite Solar Cells: From Large Grain Polycrystalline Films to Single Crystals. *Adv. Energy Mater.* **2020**, *10* (13), 1902762.

(3) Ding, C.; Jia, H.; Sun, Q.; Yao, Z.; Yang, H.; Liu, W.; Pang, X.; Li, S.; Liu, C.; Minari, T.; Chen, J.; Liu, X.; Song, Y. Wafer-Scale Single Crystals: Crystal Growth Mechanisms, Fabrication Methods, and Functional Applications. *J. Mater. Chem. C* **2021**, *9* (25), 7829−7851.

(4) Wan, Y.; Fu, J.-H.; Chuu, C.-P.; Tung, V.; Shi, Y.; Li, L.-J. Wafer-Scale Single-Orientation 2D Layers by Atomic Edge-Guided Epitaxial Growth. *Chem. Soc. Rev.* **2022**, *51* (3), 803−811.

(5) Cui, Y.; Wang, J.; Li, Y.; Wu, Y.; Been, E.; Zhang, Z.; Zhou, J.; Zhang, W.; Hwang, H. Y.; Sinclair, R.; Cui, Y. Twisted Epitaxy of Gold Nanodisks Grown Between Twisted Substrate Layers of Molybdenum Disulfide. *Science* **2024**, *383* (6679), 212−219.

(6) Panish, M. B. Molecular Beam Epitaxy. *Science* **1980**, *208* (4446), 916−922.

(7) Dong, J.; Zhang, L.; Dai, X.; Ding, F. The Epitaxy of 2D Materials Growth. *Nat. Commun.* **2020**, *11* (1), 5862.

(8) Dumcenco, D.; Ovchinnikov, D.; Marinov, K.; Lazić, P.; Gibertini, M.; Marzari, N.; Sanchez, O. L.; Kung, Y.-C.; Krasnozhon, D.; Chen, M.-W.; Bertolazzi, S.; Gillet, P.; Fontcuberta i Morral, A.; Radenovic, A.; Kis, A. Large-Area Epitaxial Monolayer MoS_2. *ACS Nano* **2015**, *9* (4), 4611−4620.

(9) Zhang, L.; Dong, J.; Ding, F. Strategies, Status, and Challenges in Wafer Scale Single Crystalline Two-Dimensional Materials Synthesis. *Chem. Rev.* **2021**, *121* (11), 6321−6372.

(10) Ji, J.; Kwak, H.-M.; Yu, J.; Park, S.; Park, J.-H.; Kim, H.; Kim, S.; Kim, S.; Lee, D.-S.; Kum, H. S. Understanding the 2D-Material and Substrate Interaction During Epitaxial Growth Towards Successful Remote Epitaxy: a Review. *Nano Converg.* **2023**, *10* (1), 19.

(11) Chand, N. MBE Growth of High-Quality GaAs. *J. Cryst. Growth.* **1989**, *97* (2), 415−429.

(12) Baek, S.-H.; Eom, C.-B. Epitaxial Integration of Perovskite-Based Multifunctional Oxides on Silicon. *Acta Mater.* **2013**, *61* (8), 2734−2750.

(13) Shan, J.; Sun, J.; Liu, Z. Chemical Vapor Deposition Synthesis of Graphene over Sapphire Substrates. *ChemNanoMat* **2021**, *7* (5), 515−525.

(14) Chen, Z.; Xie, C.; Wang, W.; Zhao, J.; Liu, B.; Shan, J.; Wang, X.; Hong, M.; Lin, L.; Huang, L.; Lin, X.; Yang, S.; Gao, X.; Zhang, Y.; Gao, P.; Novoselov, K. S.; Sun, J.; Liu, Z. Direct Growth of Wafer-Scale Highly Oriented Graphene on Sapphire. *Sci. Adv.* **2021**, *7* (47), No. eabk0115.

(15) Bae, S.-H.; Zhou, X.; Kim, S.; Lee, Y. S.; Cruz, S. S.; Kim, Y.; Hannon, J. B.; Yang, Y.; Sadana, D. K.; Ross, F. M.; Park, H.; Kim, J. Unveiling the Carrier Transport Mechanism in Epitaxial Graphene for Forming Wafer-Scale, Single-Domain Graphene. *Proc. Natl. Acad. Sci. U.S.A.* **2017**, *114* (16), 4082−4086.

(16) Xu, X.; Guo, T.; Kim, H.; Hota, M. K.; Alsaadi, R. S.; Lanza, M.; Zhang, X.; Alshareef, H. N. Growth of 2D Materials at the Wafer Scale. *Adv. Mater.* **2022**, *34* (14), 2108258.

(17) Jang, A. R.; Hong, S.; Hyun, C.; Yoon, S. I.; Kim, G.; Jeong, H. Y.; Shin, T. J.; Park, S. O.; Wong, K.; Kwak, S. K.; Park, N.; Yu, K.; Choi, E.; Mishchenko, A.; Withers, F.; Novoselov, K. S.; Lim, H.; Shin, H. S. Wafer-Scale and Wrinkle-Free Epitaxial Growth of Single-Orientated Multilayer Hexagonal Boron Nitride on Sapphire. *Nano Lett.* **2016**, *16* (5), 3360−3366.

(18) Dong, J.; Zhang, L.; Ding, F. Kinetics of Graphene and 2D Materials Growth. *Adv. Mater.* **2019**, *31* (9), 1801583.

(19) Yang, P.; Zhu, L.; Zhou, F.; Zhang, Y. Wafer-Scale Uniform Synthesis of 2D Transition Metal Dichalcogenides Single Crystals via Chemical Vapor Deposition. *Acc. Mater. Res.* **2022**, *3* (2), 161−174.

(20) Nguyen, V. L.; Lee, Y. H. Towards Wafer-Scale Monocrystalline Graphene Growth and Characterization. *Small* **2015**, *11* (29), 3512−3528.

(21) Fan, Y.; Li, L.; Yu, G.; Geng, D.; Zhang, X.; Hu, W. Recent Advances in Growth of Large-Sized 2D Single Crystals on Cu Substrates. *Adv. Mater.* **2021**, *33* (1), 2003956.

(22) Lee, Y.; Tan, H. H.; Jagadish, C.; Karuturi, S. K. Controlled Cracking for Large-Area Thin Film Exfoliation: Working Principles, Status, and Prospects. *ACS Appl. Electron. Mater.* **2021**, *3* (1), 145−162.

(23) Liu, A.-C.; Lai, Y.-Y.; Chen, H.-C.; Chiu, A.-P.; Kuo, H.-C. A Brief Overview of the Rapid Progress and Proposed Improvements in Gallium Nitride Epitaxy and Process for Third-Generation Semiconductors with Wide Bandgap. *Micromachines* **2023**, *14* (4), 764.

(24) Robinson, F.; Sethi, V.; de Groot, C. H. K.; Hector, A. L.; Huang, R.; Reid, G. Low-Pressure CVD of GeE (E = Te, Se, S) Thin Films from Alkylgermanium Chalcogenolate Precursors and Effect of Deposition Temperature on the Thermoelectric Performance of GeTe. *ACS Appl. Mater. Interfaces.* **2021**, *13* (40), 47773−47783.

(25) Bauer Pereira, P.; Sergueev, I.; Gorsse, S.; Dadda, J.; Müller, E.; Hermann, R. P. Lattice Dynamics and Structure of GeTe, SnTe and PbTe. *Phys. Status Solidi B* **2013**, *250* (7), 1300−1307.

(26) Cao, J.; Chien, S. W.; Tan, X. Y.; Tan, C. K. I.; Zhu, Q.; Wu, J.; Wang, X.; Zhao, Y.; Yang, L.; Yan, Q.; Liu, H.; Xu, J.; Suwardi, A. Realizing zT Values of 2.0 in Cubic GeTe. *ChemNanoMat* **2021**, *7* (4), 476−482.

(27) Ren, K.; Zhu, M.; Song, W.; Lv, S.; Xia, M.; Wang, Y.; Lu, Y.; Ji, Z.; Song, Z. Electrical Switching Properties and Structural Characteristics of GeSe−GeTe Films. *Nanoscale* **2019**, *11* (4), 1595−1603.

(28) Ansah-Antwi, K. K.; Soh, C. B.; Liu, H.; Chua, S. J. Growth Optimization and Characterization of GaN Epilayers on Multifaceted (111) Surfaces Etched on Si(100) Substrates. *J. Vac. Sci. Technol. A* **2015**, *33* (6), No. 061517.

(29) Kalra, G.; Murugavel, S. The Role of Atomic Vacancies on Phonon Confinement in α-GeTe. *AIP Adv.* **2015**, *5* (4), No. 047127.

(30) Pawbake, A.; Bellin, C.; Paulatto, L.; Béneut, K.; Biscaras, J.; Narayana, C.; Late, D. J.; Shukla, A. Pressure-Induced Phase Transitions in Germanium Telluride: Raman Signatures of Anharmonicity and Oxidation. *Phys. Rev. Lett.* **2019**, *122* (14), 145701.

(31) Andrikopoulos, K. S.; Yannopoulos, S. N.; Voyiatzis, G. A.; Kolobov, A. V.; Ribes, M.; Tominaga, J. Raman Scattering Study of the a-GeTe Structure and Possible Mechanism for the Amorphous to Crystal Transition. *J. Condens. Matter Phys.* **2006**, *18* (3), 965.

(32) Kim, E. T.; Lee, J. Y.; Kim, Y. T. In situ Transmission Electron Microscopy Study on the Crystallization of GeTe Binary Alloy. *Appl. Phys. Lett.* **2008**, *92* (19), 191915.

(33) Liu, J.; Liang, C.; Tian, Z.; Zhang, S.; Shao, G. Spontaneous Growth and Chemical Reduction Ability of Ge Nanoparticles. *Sci. Rep.* **2013**, *3* (1), 1741.

(34) Bedell, S. W.; Fogel, K.; Lauro, P.; Shahrjerdi, D.; Ott, J. A.; Sadana, D. Layer Transfer by Controlled Spalling. *J. Phys. D: Appl. Phys.* **2013**, *46* (15), 152002.

(35) Crouse, D.; Simon, J.; Schulte, K. L.; Young, D. L.; Ptak, A. J.; Packard, C. E. Increased Fracture Depth Range in Controlled Spalling of (100)-Oriented Germanium via Electroplating. *Thin Solid Films* **2018**, *649*, 154−159.

(36) Bedell, S. W.; Shahrjerdi, D.; Hekmatshoar, B.; Fogel, K.; Lauro, P. A.; Ott, J. A.; Sosa, N.; Sadana, D. Kerf-Less Removal of Si, Ge, and III−V Layers by Controlled Spalling to Enable Low-Cost PV Technologies. *IEEE J. Photovolt.* **2012**, *2* (2), 141−147.

(37) Luo, J. K.; Pritschow, M.; Flewitt, A. J.; Spearing, S. M.; Fleck, N. A.; Milne, W. I. Effects of Process Conditions on Properties of Electroplated Ni Thin Films for Microsystem Applications. *J. Electrochem. Soc.* **2006**, *153* (10), D155.

(38) Hohenwarter, A.; Pippan, R. Fracture Toughness Evaluation of Ultrafine-Grained Nickel. *Scr. Mater.* **2011**, *64* (10), 982−985.

(39) Bae, S.-H.; Lu, K.; Han, Y.; Kim, S.; Qiao, K.; Choi, C.; Nie, Y.; Kim, H.; Kum, H. S.; Chen, P.; Kong, W.; Kang, B.-S.; Kim, C.; Lee,

https://doi.org/10.1021/acs.nanolett.4c03127
Nano Lett. 2024, 24, 12823−12831

J.; Baek, Y.; Shim, J.; Park, J.; Joo, M.; Muller, D. A.; Lee, K.; Kim, J. Graphene-Assisted Spontaneous Relaxation Towards Dislocation-Free Heteroepitaxy. *Nat. Nanotechnol.* **2020**, *15* (4), 272−276.
(40) Zhao, Y.-F.; Guan, Z.; Zhong, N.; Yue, F.-Y.; Xiang, P.-H.; Duan, C.-G. Raman Spectra of Bulk and Few-Layer GeSe From First-Principles Calculations. *Front. Mater.* **2021**, *8*, 736057.
(41) Ye, Y.; Guo, Q.; Liu, X.; Liu, C.; Wang, J.; Liu, Y.; Qiu, J. Two-Dimensional GeSe as an Isostructural and Isoelectronic Analogue of Phosphorene: Sonication-Assisted Synthesis, Chemical Stability, and Optical Properties. *Chem. Mater.* **2017**, *29* (19), 8361−8368.
(42) Chandrasekhar, H. R.; Zwick, U. Raman Scattering and Infrared Reflectivity in GeSe. *Solid State Commun.* **1976**, *18* (11), 1509−1513.
(43) Zhang, X.; Tan, Q.-H.; Wu, J.-B.; Shi, W.; Tan, P.-H. Review on the Raman Spectroscopy of Different Types of Layered Materials. *Nanoscale* **2016**, *8* (12), 6435−6450.
(44) Chen, B.; Ruan, Y.; Li, J.; Wang, W.; Liu, X.; Cai, H.; Yao, L.; Zhang, J.-M.; Chen, S.; Chen, G. Highly Oriented GeSe Thin Film: Self-Assembly Growth via the Sandwiching Post-Annealing Treatment and Its Solar Cell Performance. *Nanoscale* **2019**, *11* (9), 3968−3978.
(45) Wuttig, M.; Yamada, N. Phase-Change Materials for Rewriteable Data Storage. *Nat. Mater.* **2007**, *6* (11), 824−832.
(46) Singh, K.; Kumari, S.; Singh, H.; Bala, N.; Singh, P.; Kumar, A.; Thakur, A. A Review on GeTe Thin Film-Based Phase-Change Materials. *Appl. Nanosci.* **2023**, *13* (1), 95−110.
(47) Zhang, W.; Ma, E. Unveiling the Structural Origin to Control Resistance Drift in Phase-Change Memory Materials. *Mater. Today* **2020**, *41*, 156−176.
(48) Lee, S.-H.; Jung, Y.; Chung, H.-S.; Jennings, A. T.; Agarwal, R. Comparative Study of Memory-Switching Phenomena in Phase Change GeTe and $Ge_2Sb_2Te_5$ Nanowire Devices. *Phys. E: Low-Dimens. Syst. Nanostructures.* **2008**, *40* (7), 2474−2480.
(49) Yu, M. J.; Son, K. R.; Khot, A. C.; Kang, D. Y.; Sung, J. H.; Jang, I. G.; Dange, Y. D.; Dongale, T. D.; Kim, T. G. Three Musketeers: Demonstration of Multilevel Memory, Selector, and Synaptic Behaviors from an Ag-GeTe Based Chalcogenide Material. *J. Mater. Res. Technol.* **2021**, *15*, 1984−1995.
(50) Bathaei, N.; Weng, B.; Sigmarsson, H. Growth Study of GeTe Phase Change Material Using Pulsed Electron-Beam Deposition. *Mater. Sci. Semicond. Process.* **2019**, *96*, 73−77.
(51) Eliseev, N. N.; Kiselev, A. V.; Ionin, V. V.; Mikhalevsky, V. A.; Burtsev, A. A.; Pankov, M. A.; Karimov, D. N.; Lotin, A. A. Wide Range Optical and Electrical Contrast Modulation by Laser-induced Phase Transitions in GeTe Thin Films. *Results Phys.* **2020**, *19*, 103466.
(52) Schenk, F. M.; Zellweger, T.; Kumaar, D.; Bošković, D.; Wintersteller, S.; Solokha, P.; De Negri, S.; Emboras, A.; Wood, V.; Yarema, M. Phase-Change Memory from Molecular Tellurides. *ACS Nano* **2024**, *18* (1), 1063−1072.
(53) Sangwan, V. K.; Hersam, M. C. Neuromorphic Nanoelectronic Materials. *Nat. Nanotechnol.* **2020**, *15* (7), 517−528.
(54) Mun, B. H.; You, B. K.; Yang, S. R.; Yoo, H. G.; Kim, J. M.; Park, W. I.; Yin, Y.; Byun, M.; Jung, Y. S.; Lee, K. J. Flexible One Diode-One Phase Change Memory Array Enabled by Block Copolymer Self-Assembly. *ACS Nano* **2015**, *9* (4), 4120−4128.

https://doi.org/10.1021/acs.nanolett.4c03127
Nano Lett. 2024, 24, 12823−12831